Macromolecules

Article

Cite This: Macromolecules 2019, 52, 819−826

pubs.acs.org/Macromolecules

Porous Polystyrene Monoliths Prepared from *in Situ* Simultaneous Interpenetrating Polymer Networks: Modulation of Morphology by Polymerization Kinetics

Petra Utroša,[†] Ema Žagar,[†] Sebastijan Kovačič,*[,†,‡] and David Pahovnik*[,†]

[†]Department of Polymer Chemistry and Technology, National Institute of Chemistry, Hajdrihova 19, 1000 Ljubljana, Slovenia

[‡]Faculty of Chemistry and Chemical Engineering, Laboratory for Organic and Polymer Chemistry and Technology, University of Maribor, Smetanova 17, 2000 Maribor, Slovenia

Supporting Information

ABSTRACT: Semi-interpenetrating polymer networks (semi-IPNs) were prepared by *in situ* simultaneous orthogonal polymerizations, where the linear poly(ε-caprolactone) (PCL) was synthesized by ring-opening polymerization of ε-caprolactone and the poly(styrene-*co*-divinylbenzene) (PS) network was formed by free-radical polymerization of styrene/divinylbenzene. Semi-IPNs were used as the precursors for the preparation of porous PS monoliths. To this end, the PCL domains were selectively removed by hydrolysis under basic conditions. By changing the amount of organocatalyst used for the ring-opening polymerization of ε-caprolactone, the relative polymerization kinetics of both monomers was varied, which has a pronounced effect on the morphology of thus-obtained PS frameworks.

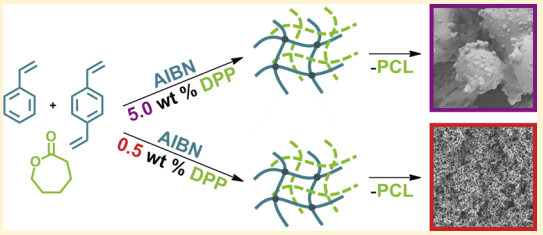

INTRODUCTION

Interpenetrating polymer networks (IPNs) consist of intertwined polymer networks that are not covalently bound to each other. Two individually cross-linked networks form a full-IPN, whereas a semi-IPN is obtained when only one of the polymeric components is cross-linked.[1,2] Entanglement of polymer chains within the IPN results in a forced miscibility of the otherwise immiscible polymers. The IPN morphology strongly depends on the synthetic conditions, affecting a phase separation process. Sequential IPNs are prepared by a two-step process, consisting of dissolving/swelling of a preformed polymer by a second monomer/cross-linker mixture that is subsequently polymerized, or by an *in situ* polymerization of a homogeneous mixture of both (macro)monomers where the polymerization of one (macro)monomer is finished before the second one starts to polymerize. On the other hand, when polymerizations of both (macro)monomers take place at the same time, an *in situ* simultaneous IPN is formed.[3] During simultaneous IPN synthesis, the rate of polymerization of each (macro)monomer can differ. The majority of literature dealing with kinetic studies comprises the IPNs prepared by free radical polymerization of vinylic monomers and step-growth polymerization of polyether polyols and isocyanates to form polyurethanes (PU).[3−8] Instead of polyether, polyisobutene,[9,10] polysiloxane,[11] and polycarbonate[12] have been applied as the components of PU, and moreover PUs were combined also with epoxy[13] or thiol−ene chemistry.[14] The effect of the order of individual network formation on the IPN morphology was studied for the *in situ* full-IPNs, consisting of polystyrene (PS) and polyisobutene-based PU.[10] For this purpose, the amount and type of the free-radical initiator were varied to form the PS network faster or slower than the PU network or to form it only after the PU network was almost fully formed. The interpenetration degree of both networks within the resulting IPNs was the highest when the PS network was formed last since in the opposite case the full (macro)-monomer conversion to PU was prevented by the PS network in the glassy state. Previous studies showed that relatively high molecular weight polyols, used for the PU network formation, enhance incompatibility between the two polymers, leading to early onset of the phase separation during IPN formation.[5,6] The onset of network gelation, which locks in the structure, also plays an important role in morphology formation of the resulting materials. In general, the PU network should form first to achieve fine interpenetration of both networks,[3,5−9,14] or the times of gelation of both networks should coincide.[11,12]

Polyurethane chemistry has also been used to cross-link the polyester polyols within the IPNs. Polyesters are particularly interesting components since they can be selectively removed from the IPNs to prepare the porous polymer monoliths, as highly desirable materials for flow-through applications in chromatographic analysis, solid phase extraction, and heterogeneous catalysis,[15,16] where a degree of phase separation determines the pore sizes.[17] *In situ* sequential full-IPNs were prepared by dissolution of polylactide (PLA) polyol in a mixture of methacrylic monomers and subsequent *in situ* cross-

Received: September 6, 2018
Revised: November 30, 2018
Published: January 11, 2019

DOI: 10.1021/acs.macromol.8b01923
Macromolecules 2019, 52, 819−826

linking of PLA to form the PU network.[18,19] Afterward, the methacrylate monomer and cross-linker were polymerized at high temperature to produce the full IPNs. Finally, the polyester network was hydrolyzed in the phosphate buffer/EtOH to obtain the porous poly(methyl methacrylate) (PMMA) frameworks. When the PLA had not been cross-linked, its removal by selective dissolution led to the porous PMMA of larger pore sizes.[20] Similar porous morphology of PMMA was obtained when poly(ε-caprolactone) (PCL) had been used as the sacrificial polyester.[21] The pore sizes of different methacrylic and styrenic frameworks, obtained after dissolution of linear PLA or after basic hydrolysis of cross-linked PLA from the IPNs, were in a range of few tens to few hundreds of nanometers.[22]

PLA has also been used as an etchable component in different copolymer systems, in which the microphase separation is a consequence of the incompatibility of covalently linked copolymer constituents. The domains and subsequently the pore sizes were in a range of few nanometers to few tens of nanometers. Nanoporous PS frameworks were prepared from the copolymer networks based on the telechelic hydroxyl-terminated PS and PLA, which were randomly end-linked with a tetrafunctional isocyanate.[23] A cross-linkable block copolymer of PLA and PS with the incorporated epoxy groups was prepared by using a macromolecular chain transfer agent (macro-CTA) based on PLA. The copolymer's disordered structure at high temperatures was kinetically trapped by a subsequent cross-linking through the epoxy groups to afford the nanoporous PS structure after PLA removal.[24] The macro-CTA based on etchable PLA was also used for polymerization of multifunctional styrene monomers. Such block copolymers were cross-linked in the course of polymerization.[25−27] Block polymerization of PLA and styrene/divinylbenzene (DVB) was performed also simultaneously from a heterofunctional initiator, so the use of macro-CTA was avoided.[28] Furthermore, a hierarchical porosity, consisting of macro- and mesopores, was obtained when the polymerization of styrene/DVB from the PLA-based macro-CTA had been performed in the presence of a nonreactive poly(ethylene oxide),[29] whereas the meso- and micropores were generated when the PS framework had been hyper-cross-linked[30] or when the sterically hindered styrene monomers had been applied.[31]

In the case of sequentially prepared semi-IPNs of PCL and cross-linked PS, the domain sizes were in a micrometer range due to the incompatibility of these two polymers.[32,33] This is expected since the blends of PCL and high molecular weight PS, prepared by extrusion[34] or solution casting,[35,36] also reveal the formation of large phase domains. Even when the PS/PCL blend (50/50) had been prepared at high temperatures to improve polymer miscibility, and subsequently quenched in liquid nitrogen to freeze-in the morphology, the blend consisted of domains with sizes in a micrometer range.[37] Nevertheless, the nanoscale blends of PCL and PS were successfully prepared by simultaneous polymerization of a mixture of monomers, wherein the individual polymerization mechanisms do not interfere;[38] however, such blends have a large tendency to phase separate over time due to absence of cross-linking.

In this work, we aimed to control the extent of phase separation of the *in situ* simultaneously prepared semi-IPNs consisted of the immiscible PCL and PS by changing their relative polymerization rate, while locking in the morphology by cross-linking the PS phase. ε-Caprolactone (CL) and styrene/DVB were polymerized *in situ* by the simultaneous orthogonal polymerizations, i.e., organocatalyzed ring-opening polymerization (ROP) and free-radical polymerization (FRP), respectively. The simultaneous formation of both polymers should improve their compatibility, leading to smaller domain sizes. After semi-IPNs formation, the PCL domains were selectively hydrolyzed to produce the porous poly(styrene-*co*-DVB) monoliths. A comprehensive study of the effect of the polymerization kinetics on the morphology of thus-obtained PS frameworks is reported herein.

EXPERIMENTAL SECTION

Materials. The chemicals 2,2′-azobis(2-methylpropionitrile) (AIBN, 98%, Fluka Chemika), 3-phenyl-1-propanol (PPA, 98%, Aldrich), diphenyl phosphate (DPP, 99%, Aldrich), and sodium hydroxide (NaOH, Honeywell) and solvents chloroform (Honeywell), methanol (Sigma-Aldrich), and toluene (Merck, anhydrous) were used as received. CL (97%, Aldrich) was dried over calcium hydride (95%, Sigma-Aldrich) overnight and distilled under vacuum. DVB (Merck) and styrene (99%, Sigma-Aldrich) were passed through a layer of active alumina (Al_2O_3, Merck) prior to use.

Methods. ^{1}H nuclear magnetic resonance (NMR) spectra were recorded on a Varian Unity Inova 300 MHz spectrometer (Varian, Inc., USA). All measurements were performed in $CDCl_3$ at room temperature in the pulse Fourier transform mode. Tetramethylsilane (TMS, $\delta = 0$) was used as an internal chemical shift standard.

Matrix-assisted laser desorption/ionization time-of-flight mass spectrometry (MALDI-TOF MS) measurements were performed on a Bruker UltrafleXtreme MALDI-TOF mass spectrometer (Bruker Daltonik, Germany). Samples were dissolved in tetrahydrofuran (THF) (10 mg mL^{-1}), and mixed with a solution of 2,5-dihydroxybenzoic acid in THF (30 mg mL^{-1}) as a matrix and sodium trifluoroacetate in THF (10 mg mL^{-1}) as a cationizer in a volume ratio of 1:10:3. A 0.4 μL of thus-prepared solution was spotted on the target plate (dried-droplet method). The reflective positive ion mode was used to acquire the samples' mass spectra. Calibration was performed externally with a mixture of PMMA standards dissolved in THF (MALDI validation set PMMA, Fluka Analytical), covering the measured molecular weight range, and using the nearest-neighbor position method.

Size-exclusion chromatography coupled to a multiangle light-scattering photometer (SEC-MALS) was performed on a modulated liquid chromatograph consisting of an Agilent Technologies 1260 series pump and a degasser (Agilent Technologies, USA) coupled to a Dawn Heleos-II multiangle light-scattering photometer with a GaAs linearly polarized laser (λ_0 = 661 nm) and to an Optilab rEX interferometric refractometer (RI), operating at the same wavelength as the photometer (both instruments are from Wyatt Technology Corp., USA). A MesoPore column (Agilent Technologies, USA) was used for sample separation by size. THF was used as the solvent (100 μL, 1 mg mL^{-1}) and eluent at a flow rate of 1 mL min^{-1}. For the data acquisition and evaluation the Astra 5.3.4 software (Wyatt Technology Corp., USA) was utilized.

Fourier-transform infrared (FT-IR) spectra were collected using a Spectrum One FT-IR spectrometer (PerkinElmer, UK). FT-IR spectra were recorded in an attenuated total reflectance (ATR) mode in a spectral range of 650−4000 cm^{-1}.

Nitrogen sorption measurements were performed on a TriStar II 3020 (Micromeritics, USA) sorption analyzer. The samples were outgassed at 40 °C. The specific surface areas (SSAs) were determined by means of the nitrogen sorption data in the relative pressure range from 0.05 to 1 using the Brunauer−Emmett−Teller (BET) method. Pore size distributions of samples were determined based on the Barrett−Joyner−Halenda (BJH) analysis of the nitrogen sorption isotherms.[39]

Scanning electron microscopy (SEM) was used to investigate the morphology of porous samples. Sample surfaces were sputtered with a

DOI: 10.1021/acs.macromol.8b01923
Macromolecules 2019, 52, 819−826

Table 1. IPN Characteristics: Remaining Monolith Mass after PCL Hydrolysis, Densities before and after Hydrolysis, Specific Surface Area, Gelation Time, and Onset of Turbidity

sample	w_{DPP} (%)	$w_{framework}$[a] (%)	ρ_1[b] (g cm^{-3})	ρ_2[c] (g cm^{-3})	SSA_{BET} (m^2 g^{-1})	gelation[d] (min)	turbidity[e] (min)
IPN_{seq}	5.0	40	0.98	0.37	4.8	12	2
$IPN_{5.0}$	5.0	40	0.90	0.31	2.9	16	10
$IPN_{2.0}$	2.0	39	0.92	0.35	4.1	22	19
$IPN_{1.5}$	1.5	40	1.02	0.44	22.7	23	22
$IPN_{1.0}$	1.0	44	1.05	0.49	47.6	27	28
$IPN_{0.5}$	0.5	46	1.06	0.50	70.3	26	45
$IPN_{0.3}$	0.3	48	1.08	0.55	46.5	29	70

[a]Remaining monolith mass after PCL hydrolysis. [b]Density determined by mass and geometry of IPN before hydrolysis. [c]Density determined by mass and geometry of IPN after PCL hydrolysis. [d]Time of gelation determined by vial inversion method. [e]Onset of turbidity determined visually.

6 nm layer of gold using a Gatan PECS 682 (Gatan, USA) sputter coater. SEM images were taken on a HR-SEM Zeiss Ultra plus instrument (Carl Zeiss, Germany).

Mercury intrusion porosimetry was performed on an AutoPore IV 9500 instrument (Micromeritics Instruments, USA). The samples were evacuated at 50 μmHg and room temperature prior to mercury intrusion. Samples were analyzed under the following parameters: contact angle = 130°, mercury surface tension = 480 mN m^{-1}, and maximum intrusion pressure = 441 MPa.

Polymerization Kinetic Studies by ^{1}H NMR. For the polymerization kinetic studies, the CL and styrene (50/50 wt %) were mixed and polymerized to prepare soluble polymers. AIBN (0.02 g, 0.12 mmol) and varied amounts of DPP were dissolved in a mixture of styrene (2.06 g, 19.8 mmol) and CL (2 mL, 18.0 mmol) and purged with nitrogen. Then, the PPA (28 μL, 0.2 mmol) was added and heated to 80 °C. Aliquots of the reaction mixture were taken at the 10 min intervals, immediately diluted with $CDCl_3$, and analyzed by ^{1}H NMR. In the same manner, the polymerization kinetics of the styrene in bulk was studied to verify whether the DPP affects the FRP kinetics.

Synthesis of PCL. PCL was synthesized by ROP of CL using DPP as an organic catalyst.[40] In a dried argon-purged flask, the DPP (0.31 g, 1.2 mmol) and CL (10 mL, 90.2 mmol) were weighed and dissolved in dry toluene (30 mL). The mixture was heated to 40 °C, and then the PPA (140 μL, 1.0 mmol) was added. The polymer was isolated after reaching ~95% monomer conversion (determined by ^{1}H NMR) by evaporating most of the solvent and precipitating the polymer with methanol at −20 °C. The product was then dried under vacuum and analyzed by ^{1}H NMR, MALDI-TOF MS, and SEC-MALS (Figures S1 and S2). M_n(NMR) = 8.7 kg mol^{-1}, M_w (SEC-MALS) = 9.8 kg mol^{-1}, and M_w/M_n = 1.13.

Synthesis of *in Situ* Simultaneous Semi-IPNs. A typical procedure for synthesis of the *in situ* simultaneous PCL/poly(styrene-*co*-DVB) (50/50 wt %) semi-IPN with a styrene/DVB composition of 90/10 mol % is as follows: AIBN (0.01 g, 0.06 mmol) and DPP (0.05 g, 0.2 mmol) were dissolved in a mixture of styrene (0.92 g, 8.8 mmol) and DVB (0.11 g, 0.9 mmol). Then, the CL (1 mL, 9.0 mmol) and PPA (14 μL, 0.1 mmol) were added to reaction mixture. After purging the mixture with nitrogen and degassing, it was kept at 80 °C overnight. Other IPNs were synthesized in a similar manner with different amounts of DPP (Table 1). For sequential synthesis, the previously prepared PCL (1.03 g) was used instead of the CL and PPA.

An onset of gelation during polymerization was determined by a vial inversion method by noting a time when the reacting liquid stopped flowing. The gel formation was additionally confirmed by submerging the selected samples in liquid nitrogen when a point of apparent gelation had been reached, followed by addition of a large amount of chloroform. The samples swelled significantly and broke apart; however, they did not dissolve completely, which clearly indicates the formation of a chemically cross-linked gel. The time of phase separation was determined visually by noting the onset of turbidity. Approximate conversions of monomers at the times of gelation and phase separation were calculated from the corresponding polymerization kinetic study, assuming the first-order kinetics.

Preparation of Porous PS Framework from the *in Situ* Simultaneous Semi-IPNs. All samples were cut into the discs of approximate height of 10 mm and diameter of 12 mm. Then, they were immersed for 6 days in a solution of 5 M NaOH in 60/40 vol % of H_2O/MeOH at 60 °C. Afterward, the samples were rinsed abundantly with a H_2O/MeOH (60/40 vol %) mixture until neutral pH, immersed in methanol overnight, and dried under vacuum.

RESULTS AND DISCUSSION

Acid-catalyzed ROP of CL using DPP as a catalyst and FRP of styrene/DVB using AIBN as an initiator were chosen as the orthogonal polymerizations for the simultaneously prepared semi-IPNs of PCL/poly(styrene-*co*-DVB) (50/50 wt %) with a styrene/DVB composition of 90/10 mol % (Scheme 1). The

Scheme 1. Schematic Presentation of the Porous PS Framework Preparation from *in Situ* Semi-IPN Synthesized by Simultaneous FRP of Styrene and DVB and ROP of CL

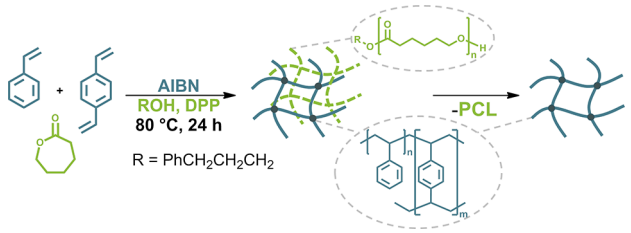

DPP catalyst offers a high degree of control over ROP of CL in solution[40] as well as in bulk.[41] Under the conditions we had used in this work, ROP and FRP did not appear to interfere with each other significantly and no copolymerization or grafting was observed. Soluble fractions obtained during extraction of the crushed IPNs in chloroform contained linear PCL chains and unreacted styrene monomer in trace amounts as determined by ^{1}H NMR (Figure S3). FT-IR spectra of the remaining cross-linked PS frameworks after removal of PCL from the IPNs by extraction showed only the bands characteristic of PS (Figure S4).

The kinetics of simultaneous ROP of CL and FRP of styrene were studied to evaluate the influence of relative polymerization rate on the IPN morphology. The polymerization rate of CL is governed by the DPP concentration, and thus it can be easily tuned. The effects of AIBN concentration, reaction temperature, and PCL molecular weight were also examined; however, these parameters offer a lesser degree of control over tuning the relative polymerization kinetics than a change in

DOI: 10.1021/acs.macromol.8b01923
Macromolecules 2019, 52, 819−826

DPP concentration. The kinetics experiments were performed in the absence of DVB cross-linker to determine the conversion of both monomers by ^{1}H NMR of aliquots taken from the reaction mixture during polymerization. The

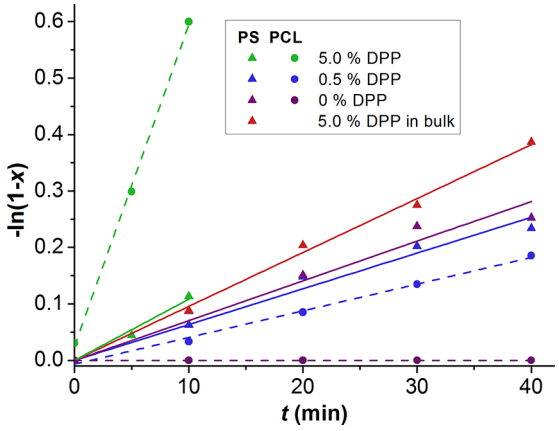

Figure 1. Kinetics of simultaneous ROP of CL (- - -) and FRP of styrene (—) in a blend of linear polymers, together with the FRP of styrene performed in bulk with added DPP.

polymerization rates of CL and styrene are not significantly affected by the addition of DVB cross-linker until the gelation point is reached; however, after the system gelation the styrene/DVB polymerization rate rapidly increases due to the increase in viscosity and entanglement degree induced by cross-linking. The conversion of CL was calculated from the integrals of signals of CL (4.22 ppm, $-CH_2CH_2O-$) and PCL (4.06 ppm, $(-CH_2CH_2O-)_n$), while the conversion of styrene was determined by comparing the integral of styrene signal (5.22 ppm, Ph−CH═C*H*H) with that of CL (4.22 ppm) at t = 0, since a broad signal of the PS aromatic ring (7.2−6.3 ppm, aromatic) is overlapping with the signals of styrene and DPP (Figure S5). The relative polymerization rate was varied by the amount of DPP added, while keeping all the other polymerization conditions constant. The polymerization rate of styrene in bulk was found to be unaffected by the addition of DPP (5.0 wt %) (Figure S6). When lowering the amount of DPP in the mixture of CL and styrene from 5.0 to 0.5 wt %, the rate of ROP of CL slowed down significantly (Figure 1). However, a small change in polymerization rate of styrene was also observed, which could be ascribed to the autoacceleration effect caused by increase in viscosity of the reaction mixture. At 5.0 wt % DPP, the CL was rapidly consumed while the polymerization kinetics of styrene resembled that in the bulk. By lowering the concentration of DPP and slowing down the PCL formation, the polymerization rate of styrene was approximately the same as if it were only diluted in CL (0 wt % DPP), indicating that the change in styrene polymerization rate could also be connected with a phase separation process and corresponding changes in the local styrene concentration.

During the IPN synthesis, the phase separation and gelation onset times were monitored. Phase separation of PCL and PS is expected due to their incompatibility (solubility parameters of PCL and PS are 20.2 and 19.3 MPa$^{1/2}$, respectively[42]).[10,43−45] The phase separation causes the sample to become opaque due to a large difference in the PCL and PS refractive indices (1.47 and 1.59 for PCL[46] and PS,[47] respectively).[9,10,20,43] Therefore, we considered the appearance of turbidity of reaction mixture as the onset of phase separation. The conversions of monomers at the times of onset of gelation and turbidity were calculated using a linear fit equation obtained from the polymerization kinetic study of the corresponding blend of linear polymers with the same amount of added DPP. The relative polymerization kinetics of the blends together with the onset points of gelation and turbidity are presented on the conversion−conversion plots in Figure 2. In terms of relative polymerization kinetics, the polymerization of CL was faster compared to that of styrene when >0.5 wt % DPP had been used. Apparently, the differences in the kinetics of polymerizations of both monomers play a fundamental role in the time order of gelation versus phase separation. At 5.0 and 2.0 wt % ($IPN_{5.0}$ and $IPN_{2.0}$) of DPP used, the PCL formed rapidly, prompting the phase separation to occur before gelation. By reduction of the DPP amount to 1.5 wt % ($IPN_{1.5}$), the turbidity appeared just before the gelation, whereas in the case of 1.0 wt % DPP ($IPN_{1.0}$) the gelation occurred just before the sample turned turbid. By reduction of

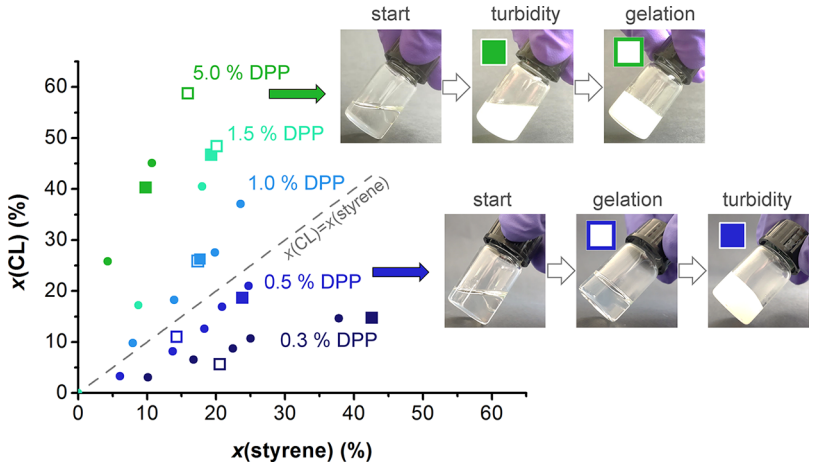

Figure 2. Conversions of CL and styrene (●) as determined by ^{1}H NMR during their simultaneous polymerization in the presence of different DPP catalyst amount, together with calculated onset of gelation (□) and phase separation (■) for each IPN. The inserted photos show that the transparent and liquid reaction mixture turned turbid first and then gelled in the case of $IPN_{5.0}$, while on the contrary the $IPN_{0.5}$ gelled before it turned turbid.

DOI: 10.1021/acs.macromol.8b01923
Macromolecules 2019, 52, 819−826

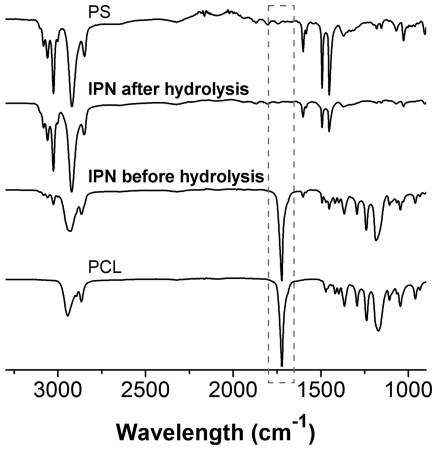

Figure 3. FT-IR spectra of IPNs before and after hydrolysis together with FT-IR spectra of PCL synthesized in solution and cross-linked PS synthesized in bulk.

the DPP further to 0.5 and 0.3 wt %, the phase separation in $IPN_{0.5}$ and $IPN_{0.3}$ occurred after gelation, since the polymerization of CL became slower than that of styrene. The gelation of the system seems to be independent of the CL polymerization rate and occurs at approximately the same conversion of styrene, while the onset of turbidity is delayed when the CL polymerizes more slowly.

The extent of phase separation in IPNs was studied after the removal of PCL within the PS networks. Extraction of PCL from the IPN monoliths by a solvent was proved to be less efficient since solvent diffusion slows down when both polymeric networks extensively interpenetrate, and furthermore, cracks occurred in the monolith as a result of swelling of PS network. To avoid significant morphological changes of the monoliths and to ensure a complete PCL removal, it was hydrolytically degraded in a basic aqueous/methanolic solution. The size and shape of the monoliths before and after PCL hydrolysis did not change significantly. The mass fractions of the samples after hydrolysis were below 50 wt % (Table 1), suggesting a complete polyester removal as supported by a disappearance of the carbonyl stretching band at 1720 cm^{-1} in the FT-IR spectra of the resulting PS frameworks (Figure 3).

Because the onset of gelation and phase separation are suggested to play a vital role in the morphology formation of IPNs,[5,6,48,49] the morphology of obtained PS frameworks was studied by SEM (Figure 4 and Figure S7). The samples where the phase separation occurred before gelation ($IPN_{5.0}$ and $IPN_{2.0}$) show much larger pores than the samples where the rate of CL polymerization was slowed down to postpone the phase separation to meet the gelation point ($IPN_{1.5}$ and $IPN_{1.0}$) or even to surpass it ($IPN_{0.5}$ and $IPN_{0.3}$). Moreover, the $IPN_{5.0}$ shows visible defects most likely due to the autoacceleration effect, resulting in lower framework density. Among the $IPN_{1.0}$, $IPN_{0.5}$, and $IPN_{0.3}$, no significant morphological differences were observed. As a reference, IPN_{seq} was prepared sequentially, where the PCL was synthesized beforehand and subsequently dissolved in a styrene/DVB mixture. To ensure the same reaction conditions for the IPN_{seq} as for the simultaneously prepared IPNs, the DPP was also added to the reaction mixture. However, the results show no influence of DPP on the morphology of IPN_{seq}

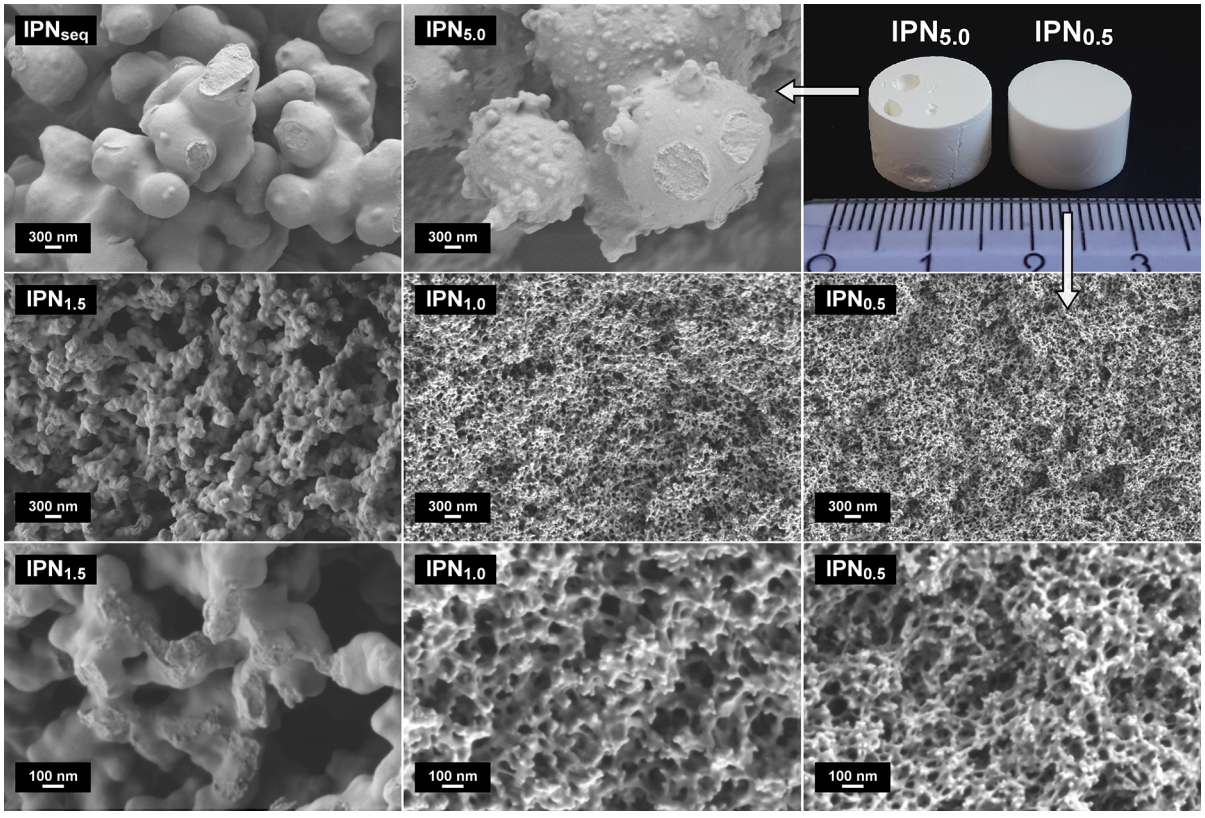

Figure 4. SEM micrographs of sequential IPN_{seq} and *in situ* simultaneous IPNs, together with a photograph of monoliths obtained after removal of PCL from IPNs. The third row represents micrographs at higher magnification of samples $IPN_{1.5}$, $IPN_{1.0}$, and $IPN_{0.5}$.

DOI: 10.1021/acs.macromol.8b01923
Macromolecules 2019, 52, 819−826

(Figure S8). The morphological features of the IPN_{seq} resemble these of the $IPN_{5.0}$, and the domain sizes correspond to those reported for the PCL/PS blends.[37] Both samples also reached the onset of turbidity before gelation, indicating that the phase separation, dictating the final morphology, is truly limited if gelation of the network occurs first. The early onset of phase separation is ascribed to the high content of PCL already at the beginning of styrene polymerization, which thus resembles early phase separation observed in the simultaneously prepared PU-based IPNs. The faster is the CL polymerization, the faster is the phase separation in the PCL/PS system and the larger are the growing PCL domains within the PS matrix, resulting in the larger pores of PS framework after PCL removal. Thus, a decrease in the pore sizes of the IPNs when going from 5 to 0.3 wt % of DPP is a result of different relative kinetics of the CL and styrene polymerizations.

Pore size distributions of PS frameworks obtained by mercury intrusion porosimetry are shown in Figure 5. The

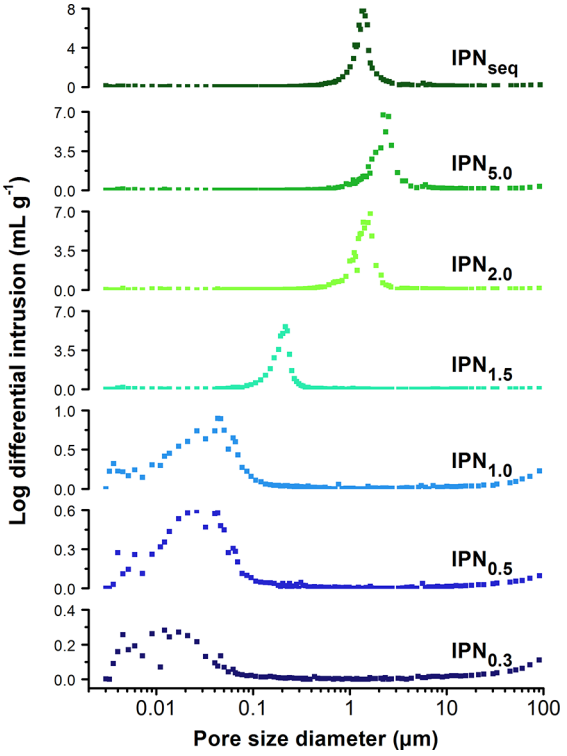

Figure 5. Pore size distributions determined by mercury intrusion porosimetry after removal of PCL from the sequential and simultaneous IPNs.

IPN_{seq}, $IPN_{5.0}$, and $IPN_{2.0}$ reveal the macroporous structures with pore sizes around 2−3 μm, which is consistent with a large domain spacing observed by SEM. The pore sizes of PS frameworks prepared by 1.0 wt % or less of DPP were shifted to much smaller pores with a majority of them smaller than 50 nm and with some also below 10 nm. The change in monoliths' pore size distribution as a function of DPP amount is rather sharp, so this transition can be observed in a fairly narrow window of relative polymerization rates only, as indicated by the $IPN_{1.5}$ monolith with the pore sizes between 100 and 400 nm.

The porous PS frameworks were further characterized by nitrogen sorption measurements. The pore size distribution as determined by BJH analysis is in relatively good agreement with data obtained by mercury intrusion porosimetry (Figure S9). SSAs were calculated using the BET theory (Table 1). The nitrogen sorption isotherms of the IPN_{seq}, $IPN_{5.0}$, and $IPN_{2.0}$ revealed no accessible micro- or mesoporosity (Figure 6

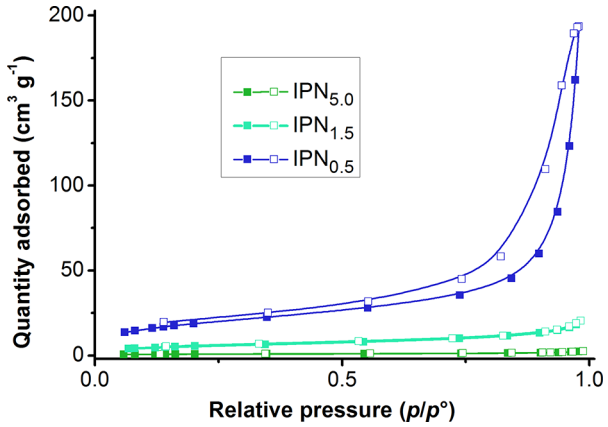

Figure 6. Isotherms from nitrogen adsorption (■) and desorption (□) measurements of the porous PS frameworks obtained after removal of PCL from IPNs.

and Figure S10). Instead, an increase of N_2 sorption uptake at $p/p_0 \approx 1$ indicates the presence of macropores, reflecting the low SSA of around 4 $m^2\ g^{-1}$. The $IPN_{1.5}$ sample shows larger SSA of 20 $m^2\ g^{-1}$ due to smaller pore sizes of 100−400 nm. On the other hand, the IPNs where the amount of DPP was ⩽1.0 wt %, the pore sizes decreased even further, with majority below 50 nm, reflecting in type IV isotherms with the hysteresis loops that are typical for mesoporous solids. In this case, the SSA increased up to ∼70 $m^2\ g^{-1}$. These results are thus in a good agreement with the mercury intrusion porosimetry data.

■ CONCLUSION

We have studied one-step, *in situ* simultaneous synthesis of semi-IPNs based on PCL and cross-linked PS with emphasis on the polymerization kinetics of CL and styrene and its effect on the IPN morphology. Semi-IPNs served us as the precursors for the preparation of porous PS frameworks, which were obtained after removal of PCL from the IPNs. By variation of the amount of the DPP organocatalyst, the relative polymerization rate was tuned, which in turn influences the time order of gelation versus phase separation. This plays a fundamental role in the final morphology of the porous network. Macroporous PS frameworks were obtained when the phase separation occurred substantially before gelation. On the contrary, when the phase separation was delayed, the PS frameworks reveal significantly smaller pores. The change in monoliths' pore size distribution as a function of DPP amount is rather sharp since the transition from ∼2 μm pore size to <80 nm was observed in a fairly narrow window of relative polymerization rates.

This work demonstrates importance of the kinetics of simultaneous and orthogonal polymerizations since it governs the time order of system gelation and phase separation, which in turn also dictates the IPN morphology and, after the removal of the PCL domains, also the pore sizes within the PS frameworks.

DOI: 10.1021/acs.macromol.8b01923
Macromolecules 2019, 52, 819−826

■ ASSOCIATED CONTENT

Supporting Information

The Supporting Information is available free of charge on the ACS Publications website at DOI: 10.1021/acs.macromol.8b01923.

^{1}H NMR, MALDI-TOF MS, and FT-IR spectra, polymerization kinetic study, SEM micrographs, BJH analyses, and nitrogen sorption isotherms (PDF)

■ AUTHOR INFORMATION

Corresponding Authors

*E-mail: sebastijan.kovacic@ki.si (S.K.).
*E-mail: david.pahovnik@ki.si (D.P.).

ORCID

Ema Žagar: 0000-0002-2694-4312
Sebastijan Kovačič: 0000-0003-2664-9791
David Pahovnik: 0000-0001-8024-8871

Notes

The authors declare no competing financial interest.

■ ACKNOWLEDGMENTS

The authors acknowledge the financial support from the Slovenian Research Agency (Research Core Funding No. P2-0145) and the Centre of Excellence—Polymer Materials and Technologies for access to the MALDI-TOF mass spectrometer.

■ REFERENCES

(1) *Interpenetrating Polymer Networks*; Klempner, D., Sperling, L. H., Utracki, L. A., Eds.; Advances in Chemistry Series; American Chemical Society: Washington, DC, 1994.

(2) *Interpenetrating Polymer Networks Around the World: Science and Engineering*; Kim, S., Sperling, L., Eds.; John Wiley & Sons: 1997.

(3) Widmaier, J.-M.; Nilly, A.; Chenal, J.-M.; Mathis, A. Dependence of the Phase Separation Process on the Relative Onset of Network Formation in Simultaneous Interpenetrating Polymer Networks. *Polymer* **2005**, *46* (10), 3318−3322.

(4) Widmaier, J.-M.; Drillières, S. Relationships between Polymerization Activating Systems and Viscoelastic Properties of the Subsequent Polyurethane/Poly(Tert-Butyl Acrylate) Interpenetrating Polymer Networks. *J. Appl. Polym. Sci.* **1997**, *63* (7), 951−958.

(5) He, X.; Widmaier, J.-M.; Meyer, G. C. Kinetics of Phase Separation in Polyurethane/Polystyrene Semi-1 Interpenetrating Polymer Networks. 1. Light Transmission Studies. *Polym. Int.* **1993**, *32* (3), 289−293.

(6) He, X.; Widmaier, J.-M.; Meyer, G. C. Kinetics of Phase Separation in Polyurethane/Polystyrene Semi-1 Interpenetrating Polymer Networks. 2. Microscopy Observations and Theoretical Approach. *Polym. Int.* **1993**, *32* (3), 295−301.

(7) Lipatov, Y. S.; Alekseeva, T. T.; Rosovitsky, V. F.; Babkina, N. V. Formation Kinetics and Viscoelastic Properties of Semi-Interpenetrating Networks Based on Crosslinked Polyurethane and Poly(Butyl Methacrylate). *Polymer* **1992**, *33* (3), 610−618.

(8) Lipatov, Y. S.; Alekseeva, T. T. Interpenetrating Polymer Networks Based on Polyurethane and Poly(Butyl Methacrylate): Interrelation Between Reaction Kinetics and Microphase Structure. *Polym. Adv. Technol.* **1996**, *7* (4), 234−246.

(9) Vancaeyzeele, C.; Fichet, O.; Boileau, S.; Teyssié, D. Polyisobutene−Poly(Methylmethacrylate) Interpenetrating Polymer Networks: Synthesis and Characterization. *Polymer* **2005**, *46* (18), 6888−6896.

(10) Vancaeyzeele, C.; Fichet, O.; Laskar, J.; Boileau, S.; Teyssié, D. Polyisobutene/Polystyrene Interpenetrating Polymer Networks: Effects of Network Formation Order and Composition on the IPN Architecture. *Polymer* **2006**, *47* (6), 2046−2060.

(11) Zhou, P.; Xu, Q.; Frisch, H. L. Kinetics of Simultaneous Interpenetrating Polymer Networks of Poly(Dimethylsiloxane-Urethane)/Poly(Methyl Methacrylate) Formation and Studies of Their Phase Morphology. *Macromolecules* **1994**, *27* (4), 938−946.

(12) Zhou, P.; Frisch, H. L. Isothermal Reaction Kinetics and Phase Behavior Analysis in the Formation of PCU/PMMA Interpenetrating Polymer Networks. *Macromolecules* **1994**, *27* (7), 1788−1794.

(13) Hua, F. J.; Hu, C. P. Interpenetrating Polymer Networks of Epoxy Resin and Urethane Acrylate Resin: 1. Kinetics of Network Formation. *Eur. Polym. J.* **1999**, *35* (1), 103−112.

(14) Fichet, O.; Vidal, F.; Laskar, J.; Teyssié, D. Polydimethylsiloxane−Cellulose Acetate Butyrate Interpenetrating Polymer Networks Synthesis and Kinetic Study. Part I. *Polymer* **2005**, *46* (1), 37−47.

(15) Xie, S.; Allington, R. W.; Fréchet, J. M. J.; Svec, F. Porous Polymer Monoliths: An Alternative to Classical Beads. In *Modern Advances in Chromatography*; Freitag, R., Ed.; Springer: Berlin, 2002; pp 87−125.

(16) Svec, F. Preparation and HPLC Applications of Rigid Macroporous Organic Polymer Monoliths. *J. Sep. Sci.* **2004**, *27* (10−11), 747−766.

(17) Grande, D. Macro-, Meso-, and Nanoporous Systems Designed from IPNs. In *Micro- and Nano-structured Interpenetrating Polymer Networks*; Thomas, S., Grande, D., Cvelbar, U., Raju, K. V. S. N., Narayan, R., Thomas, S. P., Akhina, H., Eds.; John Wiley & Sons, Inc.: Hoboken, NJ, 2016; pp 127−143.

(18) Rohman, G.; Lauprêtre, F.; Boileau, S.; Guérin, P.; Grande, D. Poly(D,L-Lactide)/Poly(Methyl Methacrylate) Interpenetrating Polymer Networks: Synthesis, Characterization, and Use as Precursors to Porous Polymeric Materials. *Polymer* **2007**, *48* (24), 7017−7028.

(19) Rohman, G.; Grande, D. Mesoporous Polymeric Materials Tailored from Oligoester-Derivatized Interpenetrating Polymer Networks. *Macromol. Symp.* **2008**, *267* (1), 21−26.

(20) Rohman, G.; Grande, D.; Lauprêtre, F.; Boileau, S.; Guérin, P. Design of Porous Polymeric Materials from Interpenetrating Polymer Networks (IPNs): Poly(DL-Lactide)/Poly(Methyl Methacrylate)-Based Semi-IPN Systems. *Macromolecules* **2005**, *38* (17), 7274−7285.

(21) Grande, D.; Rohman, G.; Millot, M.-C. Nanoporous Networks Derived from Functional Semi-Interpenetrating Polymer Networks: Preparation and Use as Ion-Exchange Chromatographic Supports. *Polym. Bull.* **2008**, *61* (1), 129−135.

(22) Grande, D.; Beurroies, I.; Denoyel, R. Novel Routes to Functional (Meso)Porous Cross-Linked Polymers Using (Semi-)Interpenetrating Polymer Networks as Nanostructured Precursors. *Macromol. Symp.* **2010**, *291*−*292* (1), 168−176.

(23) Zeng, D.; Ribbe, A.; Hayward, R. C. Anisotropic and Interconnected Nanoporous Materials from Randomly End-Linked Copolymer Networks. *Macromolecules* **2017**, *50* (12), 4668−4676.

(24) Vidil, T.; Hampu, N.; Hillmyer, M. A. Nanoporous Thermosets with Percolating Pores from Block Polymers Chemically Fixed above the Order−Disorder Transition. *ACS Cent. Sci.* **2017**, *3* (10), 1114−1120.

(25) Seo, M.; Hillmyer, M. A. Reticulated Nanoporous Polymers by Controlled Polymerization-Induced Microphase Separation. *Science* **2012**, *336* (6087), 1422−1425.

(26) Schulze, M. W.; Hillmyer, M. A. Tuning Mesoporosity in Cross-Linked Nanostructured Thermosets *via* Polymerization-Induced Microphase Separation. *Macromolecules* **2017**, *50* (3), 997−1007.

(27) Park, J.; Saba, S. A.; Hillmyer, M. A.; Kang, D.-C.; Seo, M. Effect of Homopolymer in Polymerization-Induced Microphase Separation Process. *Polymer* **2017**, *126*, 338.

(28) Seo, M.; Murphy, C. J.; Hillmyer, M. A. One-Step Synthesis of Cross-Linked Block Polymer Precursor to a Nanoporous Thermoset. *ACS Macro Lett.* **2013**, *2* (7), 617−620.

(29) Saba, S. A.; Mousavi, M. P. S.; Bühlmann, P.; Hillmyer, M. A. Hierarchically Porous Polymer Monoliths by Combining Controlled

DOI: 10.1021/acs.macromol.8b01923
Macromolecules 2019, 52, 819−826

Macro- and Microphase Separation. *J. Am. Chem. Soc.* **2015**, *137* (28), 8896−8899.
(30) Seo, M.; Kim, S.; Oh, J.; Kim, S.-J.; Hillmyer, M. A. Hierarchically Porous Polymers from Hyper-Cross-Linked Block Polymer Precursors. *J. Am. Chem. Soc.* **2015**, *137* (2), 600−603.
(31) Larsen, M. B.; Van Horn, J. D.; Wu, F.; Hillmyer, M. A. Intrinsically Hierarchical Nanoporous Polymers *via* Polymerization-Induced Microphase Separation. *Macromolecules* **2017**, *50* (11), 4363−4371.
(32) Lav, T.-X.; Carbonnier, B.; Guerrouache, M.; Grande, D. Porous Polystyrene-Based Monolithic Materials Templated by Semi-Interpenetrating Polymer Networks for Capillary Electrochromatography. *Polymer* **2010**, *51* (25), 5890−5894.
(33) Lav, T.-X.; Grande, D.; Gaillet, C.; Guerrouache, M.; Carbonnier, B. Porous Poly(Styrene-*Co*-Divinylbenzene) Neutral Monolith: From Design and Characterization to Reversed-Phase Capillary Electrochromatography Applications. *Macromol. Chem. Phys.* **2012**, *213* (1), 64−71.
(34) Mohamed, A.; Gordon, S. H.; Biresaw, G. Polycaprolactone/Polystyrene Bioblends Characterized by Thermogravimetry, Modulated Differential Scanning Calorimetry and Infrared Photoacoustic Spectroscopy. *Polym. Degrad. Stab.* **2007**, *92* (7), 1177−1185.
(35) Chun, Y. S.; Kyung, Y. J.; Jung, H. C.; Kim, W. N. Thermal and Rheological Properties of Poly(ε-Caprolactone) and Polystyrene Blends. *Polymer* **2000**, *41* (24), 8729−8733.
(36) Mamun, A.; Rahman, S. M. M.; Roland, S.; Mahmood, R. Impact of Molecular Weight on the Thermal Stability and the Miscibility of Poly(ε-Caprolactone)/Polystyrene Binary Blends. *J. Polym. Environ.* **2018**, *26* (8), 3511−3519.
(37) Sarazin, P.; Favis, B. D. Influence of Temperature-Induced Coalescence Effects on Co-Continuous Morphology in Poly(ε-Caprolactone)/Polystyrene Blends. *Polymer* **2005**, *46* (16), 5966−5978.
(38) Zinck, P.; Brachais, C.; Finot, E.; Barbier-Baudry, D. Nanoscale Blends between Immiscible Polymers via Simultaneous Non-Interfering Polymerisation. *Macromol. Chem. Phys.* **2005**, *206* (5), 553−558.
(39) Barrett, E. P.; Joyner, L. G.; Halenda, P. P. The Determination of Pore Volume and Area Distributions in Porous Substances. I. Computations from Nitrogen Isotherms. *J. Am. Chem. Soc.* **1951**, *73* (1), 373−380.
(40) Makiguchi, K.; Satoh, T.; Kakuchi, T. Diphenyl Phosphate as an Efficient Cationic Organocatalyst for Controlled/Living Ring-Opening Polymerization of δ-Valerolactone and ε-Caprolactone. *Macromolecules* **2011**, *44* (7), 1999−2005.
(41) Saito, T.; Aizawa, Y.; Tajima, K.; Isono, T.; Satoh, T. Organophosphate-Catalyzed Bulk Ring-Opening Polymerization as an Environmentally Benign Route Leading to Block Copolyesters, End-Functionalized Polyesters, and Polyester-Based Polyurethane. *Polym. Chem.* **2015**, *6* (24), 4374−4384.
(42) *Hansen Solubility Parameters: A User's Handbook*, 2nd ed.; Taylor and Francis: Hoboken, NJ, 2012.
(43) Vancaeyzeele, C.; Fichet, O.; Amana, B.; Boileau, S.; Teyssié, D. Polyisobutene/Polycyclohexyl Methacrylate Interpenetrating Polymer Networks. *Polymer* **2006**, *47* (17), 6048−6056.
(44) Frisch, H. L. Factors Affecting the Miscibility of Simultaneous IPNs and Pseudo-IPNs. *Prog. Org. Coat.* **1996**, *27* (1−4), 67−72.
(45) Binder, K.; Frisch, H. L. Phase Stability of Weakly Crosslinked Interpenetrating Polymer Networks. *J. Chem. Phys.* **1984**, *81* (4), 2126−2136.
(46) Othman, R.; Vladisavljević, G. T.; Nagy, Z. K.; Holdich, R. G. Encapsulation and Controlled Release of Rapamycin from Polycaprolactone Nanoparticles Prepared by Membrane Micromixing Combined with Antisolvent Precipitation. *Langmuir* **2016**, *32* (41), 10685−10693.
(47) *Polymer Handbook*, 4th ed.; Brandrup, J., Immergut, E. H., Grulke, E. A., Eds.; Wiley: New York, 2004.
(48) Widmaier, J.-M. Microphase Separation during the Concurrent Formation of Two Polymer Networks. *Macromol. Symp.* **1995**, *93* (1), 179−186.
(49) Mishra, V.; Du Prez, F. E.; Gosen, E.; Goethals, E. J.; Sperling, L. H. Simultaneous Interpenetrating Networks of a Polyurethane and Poly(Methyl Methacrylate). I. Metastable Phase Diagrams. *J. Appl. Polym. Sci.* **1995**, *58* (2), 331−346.

DOI: 10.1021/acs.macromol.8b01923
Macromolecules 2019, 52, 819−826